Thin Solid Films 520 (2012) 7224–7229

Contents lists available at SciVerse ScienceDirect

Thin Solid Films

journal homepage: www.elsevier.com/locate/tsf

Laser induced changes of $As_{50}Se_{50}$ nanolayers studied by synchrotron radiation photoelectron spectroscopy

O. Kondrat [a,*], N. Popovich [a], R. Holomb [a], V. Mitsa [a], V. Lyamayev [b], N. Tsud [c], V. Cháb [d], V. Matolín [c], K.C. Prince [b,e]

[a] Institute of Solid State Physics and Chemistry, Uzhhorod National University, Pidhirna str., 46, 88000 Uzhhorod, Ukraine
[b] Sincrotrone Trieste S.C.p.A., Strada Statale 14, km 163.5, 34149 Basovizza, Trieste, Italy
[c] Charles University, Faculty of Mathematics and Physics, Department of Surface and Plasma Science, V Holešovičkách 2, 18000 Prague 8, Czech Republic
[d] Institute of Physics, Academy of Sciences of the Czech Republic, Cukrovarnická 10, 16253 Prague 6, Czech Republic
[e] IOM, 34149 Basovizza, Trieste, Italy

ARTICLE INFO

Article history:
Received 3 January 2012
Received in revised form 25 July 2012
Accepted 26 July 2012
Available online 2 August 2012

Keywords:
Chalcogenide glass
$As_{50}Se_{50}$
Photostructural changes
Photoelectron spectroscopy

ABSTRACT

The influence of near bandgap laser irradiation on the structure of the $As_{50}Se_{50}$ thin film has been investigated by synchrotron radiation photoelectron spectroscopy. The As 3d and Se 3d photoemission peaks of the irradiated sample show significant differences in shapes and positions in comparison with those obtained for non-irradiated amorphous film. The experimental data processing and quantifications are performed analyzing As 3d and Se 3d core-level components obtained by curve fitting. The relative contribution of the As and Se atoms in different chemical states to the whole As 3d and Se 3d signal, its structural origins as well as their relation to the $As_{50}Se_{50}$ nanolayers structure before and after laser irradiation is analyzed and discussed in detail.

1. Introduction

Amorphous chalcogenides represent a class of disordered semiconducting materials obtained by the combination of one or more chalcogen elements (typically S, Se, Te) with other elements typically As, Ge, Sb etc. They have been of great interest due to their remarkable structural, electronic and optical properties and have a wide range of potential applications [1]. Since their discovery, amorphous chalcogenides have stood out as the materials of choice for infrared (IR) optics because of their excellent optical transparency. Chalcogenide glasses (ChG) are also known for being sensitive to near-bandgap light, which produces several types of photoinduced changes in structure and properties [2,3]. These changes can be permanent, metastable or temporary depending on light exposure. Numerous interesting applications have been developed and designed based on the light sensitive properties of non-crystalline chalcogenides, especially in amorphous thin film form [4–7]. Also, we note that due to surface effects the processes of the photoinduced structural changes in thin films can be significantly different from those occurring in bulk glasses [8]. Photosensitivity is a key feature of chalcogenide glasses for phase-change memory, direct waveguide and grating writing. The high IR transparency of ChG based fibers can be used for transmitting high power IR light. Large refractive indices and third-order optical nonlinearities exhibited by chalcogenide glasses make them attractive and among the best candidates as photonic devices for ultrafast all-optical switching and data processing [9]. The effect of reversible anisotropic volume change induced by polarized light, discovered by Krecmer et al. in $As_{50}Se_{50}$ thin films, can also be used for direct opto-mechanical transformations [10]. The observed peculiarities in amorphous chalcogenides are first of all related to their structure at the nanoscale. Therefore they are interesting as model objects too, and have been intensively studied for better understanding of ordering and self-organization in amorphous materials.

Numerous experimental techniques have been used to investigate and characterize the structure of non-crystalline chalcogenides at the nanoscale, including conventional diffraction methods, inelastic neutron and Raman scattering [11]. Structural modeling, *i.e.* molecular dynamics (MD) simulations and *ab initio* calculations have also been applied to unambiguous interpretation of the experimental results [12]. For instance, Raman spectroscopy used together with *ab initio* calculations elucidated the structure of glassy As–S and Ge–S chalcogenides at the atomic scale as well as to study photo-induced transformations [13]. Theoretical and experimental investigations during the last few years have shown that two- and three-component chalcogenide glassy semiconductors, produced as continuous media, contain a considerably wider variety of basic structural units (s.u.) than their crystal analogs. The majority of s.u. consists of medium-range ordered groups or clusters with different

* Corresponding author at: Institute of Solid State Physics and Chemistry, Uzhhrord National University, Voloshin 54 str., Uzhhorod, 88000, Ukraine. Tel.: +380 31 22 33020; fax: +380 31 22 32339.
E-mail address: kon_alex@gala.net (O. Kondrat).

0040-6090/$ – see front matter © 2012 Elsevier B.V. All rights reserved.
http://dx.doi.org/10.1016/j.tsf.2012.07.116

geometry, depending on the concentration of additives and fabrication method [14]. The ordering geometry of these groups in bulk glasses and films determines their physical properties [15].

The structural information obtained from the Raman spectra of the binary As – Se system is limited. This is due to the similarity of the As and Se atomic masses, resulting in overlapping of the Raman active modes characteristic of As – As, As – Se and Se – Se stretching vibrations. On the other hand, the local structure of amorphous and glassy chalcogenides in the first coordination sphere (*i.e.* short range order) can be investigated by using high resolution X-ray photoelectron spectroscopy [16,17], because the core level binding energy gives direct information on the chemical state of the atom, and therefore its bonding. The obtained direct structural information could be extremely useful for further theoretical *ab initio* and MD structural modeling and interpretation of spectroscopic results, extending our knowledge about s.u. to larger scales (*i.e.* medium range order).

The main objectives of the present work were: to investigate the nature of light-induced structural changes of amorphous $As_{50}Se_{50}$ thin films at the atomic scale (i), to determine the effect of air on surface structure (ii), and finally to compare the types and concentrations of different structural units in the $As_{50}Se_{50}$ film before and after laser irradiation by means of synchrotron radiation photoelectron spectroscopy (SRPES) (iii). For these purposes, SRPES spectra of amorphous and laser irradiated $As_{50}Se_{50}$ films were measured. The As 3d and Se 3d core level spectra were deconvoluted into the individual components using an iterative least-squares fitting procedure. The structural origin, the contribution of each component to the experimental photoemission spectrum and its connection to the local structure of the films as well as their changes induced by air and/or laser irradiation are analyzed and discussed in detail.

2. Experimental details

The bulk $As_{50}Se_{50}$ samples were prepared by the conventional melt-quenching route in evacuated quartz ampoules from a mixture of high purity 99.999% As and Se precursors. The furnace was rocked to obtain the most homogeneous melt. All ingots were quenched by switching off the furnace. Amorphous $As_{50}Se_{50}$ thin films with thickness of about 500 Å were prepared by thermal evaporation of bulk glass onto (100) silicon crystal wafer substrates. For the laser irradiation experiment, the amorphous $As_{50}Se_{50}$ thin film was covered by aluminum foil with a hole of ~3 mm diameter. The irradiation was carried out in air at room temperature for ~3 h by a He–Ne (632.8 nm) laser of 50 mW/cm^2 intensity. The laser intensity and exposure were chosen based on our previous studies of As–Se glasses by means of Raman spectroscopy.

Photoemission measurements were performed at the Materials Science Beamline of the Elettra Synchrotron light source (Trieste, Italy). The surfaces of the films were cleaned by Ar-ion sputtering. To minimize possible changes of surface As/Se stoichiometry due to Ar-ion bombardment, low sputtering exposure (500 V, 5 min) was used, enough for removal of only the top impurity overlayer. The photoemission spectra were taken using synchrotron light with photon energy 450 eV for As 3d, Se 3d, C 1s core levels and 600 eV for O 1s core level at normal emission geometry. The As 3d, Se 3d, C 1s and O 1s core level spectra of as-prepared and laser irradiated $As_{50}Se_{50}$ films were measured with resolution of 0.5 eV. Photoemission spectra were recorded using the beamline's PHOIBOS 150 multi-channel hemispherical analyzer, with pass energy of 10 eV. The SRPES peak intensities were normalized to the incident photon flux. Charging was observed for all samples. For the correction of this effect, the binding energy (BE) of a surface impurity C 1s signal (284.8 eV) was used which was crosschecked using the BE of the Se $3d_{5/2}$ bulk signal (54.7 eV) [16]. The charging potential was very slightly (~0.1 eV) different for films before and after irradiation, indicating a minor change in conductivity. For the amorphous and cleaned $As_{50}Se_{50}$ film we did not observe the usual signs of significant charging, which are shoulders on the high BE side of Se 3d core level spectra and broadening of the core level peaks (see Fig. 1B). The same is true for the measured As 3d core level of irradiated $As_{50}Se_{50}$ film (Fig. 2A and B). Also, we checked the evolution of Se 3d and As 3d core level spectra under X-rays during the time necessary for recording the spectra and we found that the position and shape of the spectral features is stable with time. The measured intensities of synchrotron radiation excited As 3d, Se 3d, O 1s, and C 1s core level spectra were normalized by the corresponding atomic photoionization cross-sections [17,18].

The Se 3d and As 3d core level peaks were fitted using a Voigt function with subtraction of a Shirley type background to yield peak position and intensity. The statistical branching ratio of 3:2 was used for the $3d_{5/2}$ and $3d_{3/2}$ spin-orbit split peaks. Doublet separations of 0.69 and 0.86 eV were used for As 3d and Se 3d core levels, respectively. The full-width-at-half-maximum (FWHM) during the fit was set to the same value for each doublet with the same origin while it was kept free for all individual components. The binding energy and the intensity of the $3d_{5/2}$ peaks of each doublet were allowed to vary freely and independently of each other.

3. Results and discussion

3.1. SRPES spectra of As 3d and Se 3d core levels of amorphous and irradiated films

Fig. 1 shows the Se 3d and As 3d core level spectra of amorphous exposed to air (A) and Ar-ion cleaned (B) $As_{50}Se_{50}$ films together with the results of curve fitting. Comparison of the spectra demonstrates that the peak intensities and shapes are different for amorphous and Ar-ion cleaned $As_{50}Se_{50}$ films while the BEs of peak components are nearly the same. Detailed analysis of the Se 3d core levels shows that the best fit is obtained when three components (spin-orbit split doublets) for the uncleaned amorphous sample and one component for the cleaned sample were used (Fig. 1, left, A and B, respectively). As expected, the main component in the Se 3d spectra at ~54.7 eV (peak 1) of cleaned $As_{50}Se_{50}$ film is connected with As – **Se** – As s.u. [16]. Two additional components observed in Se 3d spectra of the uncleaned sample were found at ~55.1 eV (peak 2) and ~55.6 eV (peak 3) BE with respect to the main one. According to published data, they can be assigned to Se-rich As – **Se** – Se and Se – **Se** – Se s.u., respectively [19]. Therefore, from the analysis of Se 3d spectra of amorphous $As_{50}Se_{50}$ films exposed to air even Se – **Se** – Se coordination geometry can be realized. Also, the increases in BE can be attributed to the formation of Se – C bonds at the interface.

To obtain a good fit of the As 3d spectra, two components for the amorphous uncleaned sample and three components for the Ar-ion cleaned sample were used (Fig. 1, right, A and B, respectively). Two of them were assigned to arsenic bonded to two selenium and one arsenic atoms (2Se – **As** – As, ~42.5 eV, peak2) and arsenic bonded to three selenium atoms (**As** – 3Se, ~42.9 eV, peak 3) s.u.; these energies are in good agreement with values reported for known materials with corresponding arsenic chemical coordination: As_4Se_4, and As_2Se_3, respectively [19–23]. We suppose that the peak at ~42.1 eV (peak 1) originates from a 2As – **As** – Se s.u. Thus, three types of arsenic coordination may be resolved and used to explore the structure of $As_{50}Se_{50}$ nanolayers at the atomic scale.

The Se 3d and As 3d SRPES core level spectra of laser irradiated $As_{50}Se_{50}$ films before and after Ar-ion sputtering and the results of peak fitting are shown in Fig. 2. For clarity, the labeling of components with different structural origin was kept identical to those obtained for amorphous samples. The relative intensity of SRPES peaks shows significant variations in comparison with the amorphous sample while their BEs vary only negligibly. In contrast to the data obtained for the amorphous sample the Se 3d core level of the irradiated and cleaned $As_{50}Se_{50}$ film is fitted well using two components with BE at

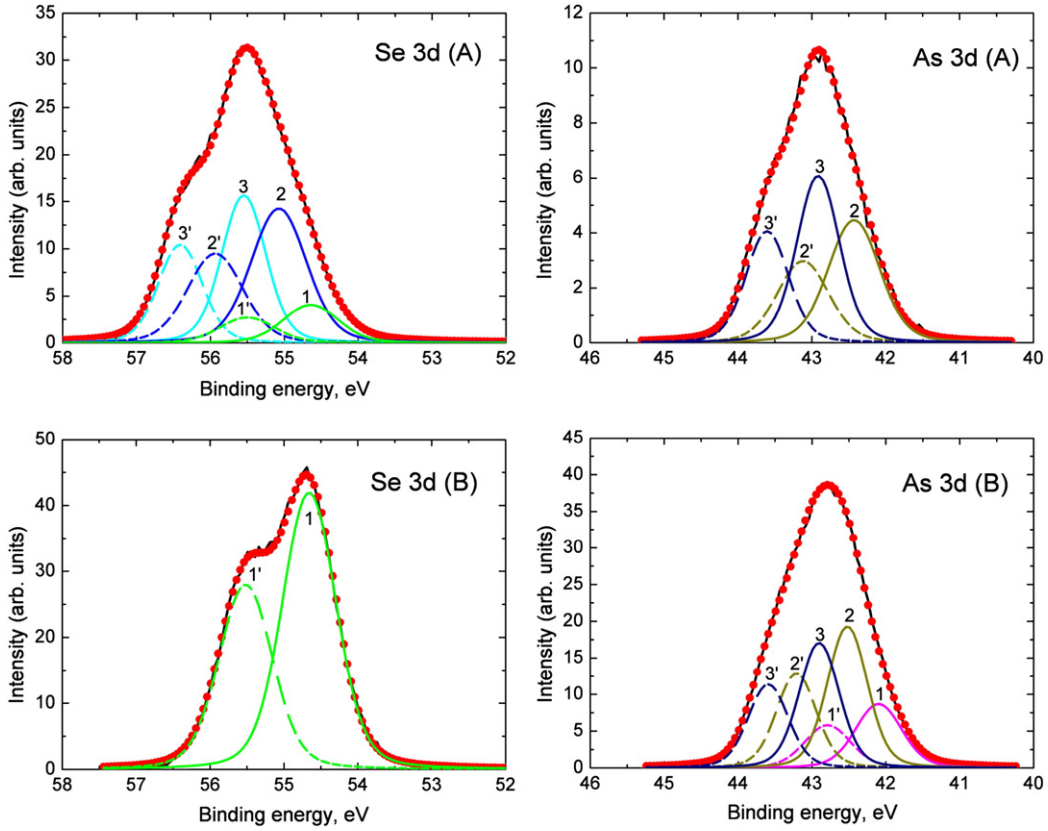

Fig. 1. Se 3d and As 3d core level spectra of amorphous exposed to air (A) and Ar-ion cleaned (B) $As_{50}Se_{50}$ films (black dots) together with the results of curve fitting (red solid line). Se 3d peak components were identified as As – **Se** – As (1), As – **Se** – Se (2) and Se – **Se** – Se (3); for As 3d — Se – **As** – 2As (1), 2Se – **As** – As (2) and **As** – 3Se (3). Continuous and dotted lines denote $3d_{5/2}$ and $3d_{3/2}$ peaks, respectively. Photon energy 450 eV.

~54.7 and 55.2 eV (peak 1 and peak 2 in Fig. 2B) corresponding to the As – **Se** – As and As – **Se** – Se s.u., respectively.

An essential change was observed in the As 3d SRPES core level spectra of the laser irradiated samples. For the irradiated $As_{50}Se_{50}$ film, the As 3d spectra were fitted using one component only (**As** – 3Se s.u.) and no **As**-rich units (Se – **As** – 2As, 2Se – **As** – As) contribution (peaks 1 and 2) was detected (Fig. 2A and B). The analysis of peak intensities of As 3d, Se 3d SRPES spectra of amorphous and irradiated $As_{50}Se_{50}$ film before and after Ar-ion sputtering is shown in Table 1. The detailed analysis of observed changes will be discussed in next two paragraphs.

3.2. Stoichiometry changes of amorphous $As_{50}Se_{50}$ surface nanolayers: effect of air and Ar-ion sputtering

It is evident from Table 1 that in the amorphous uncleaned sample exposed to air, the stoichiometry is significantly different from that of bulk $As_{50}Se_{50}$ glass. The As-to-Se (As/Se) ratio calculated from SRPES data is 0.29. Other authors reported similar losses of As immediately after an As–Se sample was exposed to air [24–27]. Antoine et al. observed that the As/Se ratio decreases immediately after the sample was oxidized (exposed to O_2) and further light illumination leads to only very small changes in the As/Se ratio [28,29]. They pointed out that the reduced amount of arsenic could be due to preferential sublimation of As atoms under ultra high vacuum. Some authors relate the change of the As/Se ratio to desorption of relatively more volatile arsenic oxides *i.e.* As_2O_3 actively formed on the surface during laser irradiation [29]. Such interpretations, however, do not correlate with the interesting observation of the As/Se ratio recovering after thermal treatment of the material [26]. An alternative idea has been proposed by Krishnaswami et al. who pointed out that light induced changes of the surface composition could be due to preferential segregation of selenium from the bulk to the surface [24]. Their suggestion is based on different formation energies for Se and As site defects, resulting in movement of atoms that easily create defects (Se) to the surface. In this case, if the surface composition of an exposed to air film is enriched by Se, then one would expect to observe As-rich layers deeper in the solid. Therefore, additional investigation is required to provide direct confirmation of either segregation or other processes taking place during exposure to air. Our component analysis for the Se 3d spectra shows the presence of a large amount of Se – Se-bonds. On the other hand, we have not detected a contribution of oxidized arsenic (As_2O_3) in the experimental As 3d peak for this sample. Such a contribution is expected when the As-rich sample is exposed to air [30]. Therefore, the segregation of Se can be due to evaporation of more volatile arsenic trioxide resulting in drastic losses of As from the surface.

The concentration of As increases to 45.3% in Ar-ion sputtered amorphous $As_{50}Se_{50}$ film (Table 1) which is still less than the source glass. In addition there are no defect Se – Se bonds found in the Se 3d spectra of the Ar-ion cleaned surface (Fig. 1B). The absence of As-rich ($x>50$) layers in the bulk leads us to conclude that As_2O_3 volatility is the main feature causing the decreases of arsenic concentration.

3.3. Component analysis and the laser induced transformations

Additional changes in surface stoichiometry and local chemical coordination were induced by near bandgap laser irradiation. For the irradiated uncleaned sample, small increases in As content by about 5% in

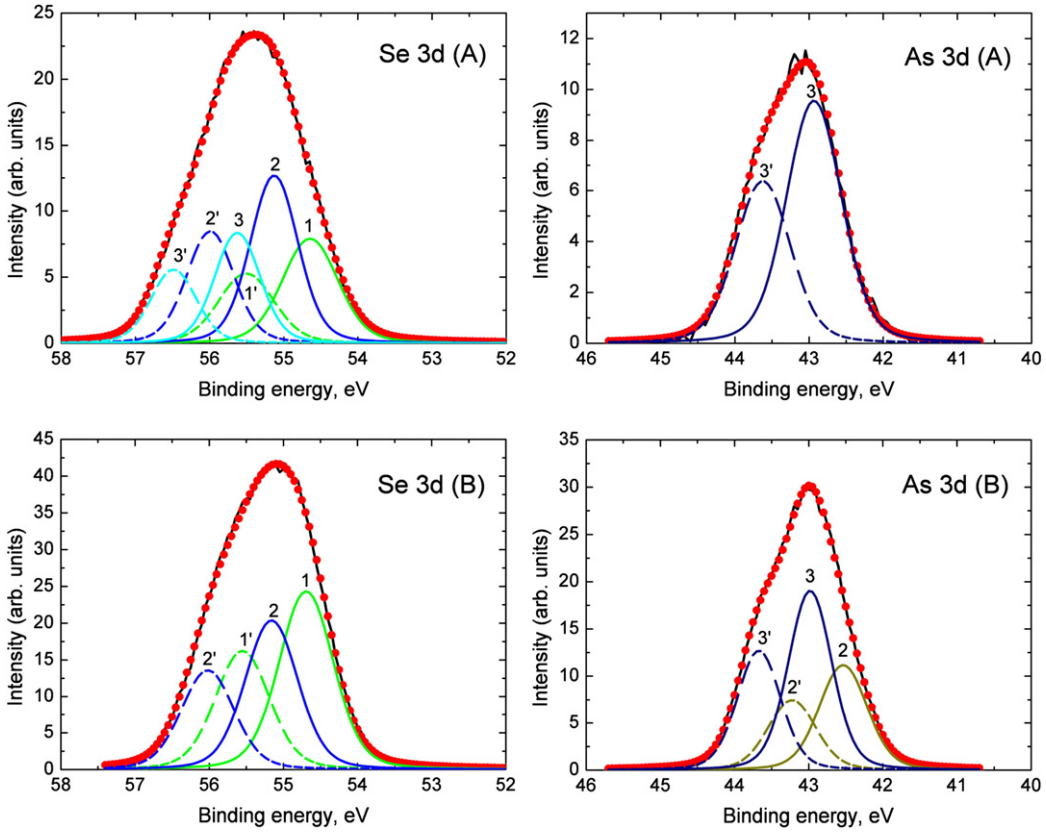

Fig. 2. Se 3d and As 3d SRPES core level spectra of laser irradiated $As_{50}Se_{50}$ films before (A) and after Ar-ion sputtering (B) (black dots) together with the results of curve fitting (red solid line). The Se 3d peak components were identified as As – **Se** – As (1), As – **Se** – Se (2) and Se – **Se** – Se (3); for As 3d — 2Se – **As** – As (2) and **As** – 3Se (3). Continuous and dotted lines denote $3d_{5/2}$ and $3d_{3/2}$ peaks, respectively. Photon energy 450 eV.

comparison with the amorphous sample were observed (Table 1). This observation is in contrast with other data observed for an annealed As_2Se_3 sample, illuminated in an inert atmosphere [26]. On the other hand Antoine et al. [29] observed As enrichment in $As_{36}Se_{64}$ film and pointed out that this is due to the loss of Se from the surface of the film. Our results support this interpretation: the comparison of Se 3d and As 3d spectra of uncleaned $As_{50}Se_{50}$ film shows that the laser illumination led to a relative increase of As 3d peak area (about +7%) and simultaneous decrease of the Se 3d peak area by about −21%.

The BE, FWHM and relative areas of individual components obtained by curve fitting of SRPES data of films before and after Ar-ion sputtering are summarized in Tables 2 and 3, respectively. The As 3d component analysis shows that the structure of the amorphous $As_{50}Se_{50}$ film exposed to air consists of two As-centered s.u. with the main contribution of **As** – 3Se (53%) and 2Se – **As** – As (47%) (Table 2). Therefore, even after exposure of the film to ambient conditions the two structural configurations are possible. This may imply that the pyramidal base $AsSe_3$ structures and the so called realgar (r) cage-like As_4Se_4 (isostructural with r-As_4S_4) molecules, whose building blocks consist solely of 2Se – **As** – As s.u., are the main structural motifs of the amorphous $As_{50}Se_{50}$ film.

Table 1
Atomic concentrations and As/Se ratio of non-irradiated and irradiated $As_{50}Se_{50}$ film calculated from SRPES data.

$As_{50}Se_{50}$ sample		As, %	Se, %	As/Se
Before Ar-ion treatment	Amorphous	22.3	77.7	0.29
	Irradiated	27.0	73.0	0.37
After Ar-ion treatment	Amorphous	45.3	54.7	0.83
	Irradiated	36.0	64.0	0.56

SRPES spectra of the Se 3d core level of the amorphous uncleaned $As_{50}Se_{50}$ film contain three types of Se core states corresponding to the As – **Se** – As (13%), Se – **Se** – As (46%) and Se – **Se** – Se (41%) s.u. (Table 2).

Drastic changes of the contributions of the components in the As 3d and Se 3d core level spectra after laser irradiation of the $As_{50}Se_{50}$ film were observed (Fig. 2). Since the BE of the peak components was only slightly changed after laser treatment their assignment can be considered as the same.

In the As 3d spectrum of the irradiated $As_{50}Se_{50}$ film (Fig. 2A), the As-rich 2Se – **As** – As component disappears compared with the corresponding spectra of the amorphous sample. Therefore, the surface layers of the $As_{50}Se_{50}$ film after laser irradiation contain only one As-centered building block **As** – 3Se s.u. as the main component

Table 2
Binding energies (BE, eV) and FWHM (eV) of individual components determined from curve fitting of Se 3d and As 3d SRPES spectra of $As_{50}Se_{50}$ films before Ar-ion treatment and their contribution (Area, %). The main ($3d_{5/2}$) peak of each doublet is considered.

Deconvoluted peak number	Core level/ component	Amorphous sample			Irradiated sample		
		BE	FWHM	Area, %	BE	FWHM	Area, %
	Se 3d:						
Peak 1	As – **Se** – As	54.64	0.88	13	54.64	0.88	31
Peak 2	As – **Se** – Se	55.07	0.89	46	55.13	0.76	43
Peak 3	Se – **Se** – Se	55.55	0.70	41	55.62	0.72	26
	As 3d:						
Peak 1	2Se – **As** – As	42.42	0.82	47	–	–	–
Peak 2	**As** – 3Se	42.91	0.68	53	42.93	0.88	100

Table 3
Binding energies (BE, eV) and FWHM (eV) of individual components determined from curve fitting of Se 3d and As 3d SRPES spectra of $As_{50}Se_{50}$ films after Ar-ion treatment and their contribution (Area, %). The main ($3d_{5/2}$) peak of each doublet is considered.

Deconvoluted peak number	Core level/ component	Amorphous sample			Irradiated sample		
		BE	FWHM	Area, %	BE	FWHM	Area, %
	Se 3d:						
Peak 1	As – **Se** – As	54.66	0.85	100	54.60	0.89	55
Peak 2	As – **Se** – Se	–	–	–	55.05	0.88	45
	As 3d:						
Peak 1	Se – **As** – 2As	42.10	0.73	22	–	–	–
Peak 2	2Se – **As** – As	42.52	0.64	41	42.53	0.76	39
Peak 3	**As** – 3Se	42.90	0.64	37	42.98	0.69	61

(100%) (Table 2). A similar situation in the As 3d spectra of irradiated $As_{50}Se_{50}$ after Ar-ion treatment was observed: in contrast to As 3d core level spectra of cleaned amorphous sample (Fig. 1B), the As rich Se – **As** – 2As component has disappeared (Fig. 2B). This indicates that laser induced As – As-bond breaking is taking place in the bulk too.

Taking into account that the realgar-like As_4Se_4 molecules (isostructural with r-As_4S_4) consist solely of 2Se – **As** – As s.u. and their pararealgar form is constructed from a mixture of **As** – 3Se, Se – **As** – 2As, and 2Se – **As** – As s.u., the photoelectron spectroscopy results do not confirm that a laser induced realgar-to-pararealgar transformation is taking place. Therefore, there is no direct evidence for such a photochemical molecular transformation in $As_{50}Se_{50}$ thin film [31], as was established in crystalline As_4S_4 [32,33] and amorphous As_xS_{100-x} chalcogenides enriched by arsenic ($x > 40$) [34,35].

Further analysis of the Se 3d peak components (Table 2) of the irradiated film shows the drastic changes in component concentrations in comparison with the amorphous sample. For the illuminated sample, the concentrations of As – **Se** – As, As – **Se** – Se and Se – **Se** – Se s.u. were calculated to be 31%, 43% and 26% (Table 2). As can be seen from Figs. 1A and 2A, the decreasing concentration of Se – **Se** – Se s.u. (from 41% to 26%) is accompanied by a simultaneous increase of As – **Se** – As s.u. concentration from 13% to 31%. Similar laser stimulated bond breaking and new bond formations was shown in [8]. The increase in concentration of As – **Se** – As s.u. after laser irradiation correlates with the mentioned stoichiometry changes. Also, the laser illumination leads to redistribution of intensities between Se-rich components (Figs. 1A and 2A). Detailed analysis the Se 3d spectrum of the cleaned irradiated film (Table 3) shows an absence of Se-rich Se – **Se** – Se component in comparison with the uncleaned sample, accompanied by an increase of the As – **Se** – As concentration. The comparison of Se 3d spectra of cleaned amorphous and irradiated samples (Figs. 1B and 2B) leads to the conclusion that laser illumination results in formation of additional Se – **Se** – As s.u. in the bulk. However, the composition of irradiated and cleaned $As_{50}Se_{50}$ film, calculated at 36.0% As, is found to be less than that calculated for the amorphous cleaned sample (45.3%) (Table 1). Such observations indicate that the above mentioned photo-induced enrichment by As cannot solely be explained by the loss of selenium from the surface.

Our results show that the laser illumination stimulates diffusion of arsenic atoms from near surface layers to the top (decreasing concentration gradient) through the bond breaking (As – As) and bond switching (As – Se) mechanisms. This model can explain the difference of As concentrations in Ar-ion cleaned $As_{50}Se_{50}$ nanolayers before and after laser irradiation.

4. Conclusions

The local structural changes of $As_{50}Se_{50}$ nanolayers induced by air and near bandgap laser irradiation have been studied in detail using synchrotron radiation photoelectron spectroscopy. The results, together with spectral analysis of the photoinduced processes, lead to the following conclusions. The crucial changes of surface stoichiometry of amorphous $As_{50}Se_{50}$ film exposed to air are found to be mainly due to arsenic oxidization and the evaporation of more volatile As_2O_3. This leads to the Se enrichment of the surface layer and formation of a gradient of composition. Near bandgap laser illumination of the $As_{50}Se_{50}$ thin film stimulates the diffusion process, decreasing the composition gradient. The component analysis of the As3d and Se3d spectra shows that the induced bond breaking (As – As) and bond switching (As – Se) mechanism are responsible for such processes. Near bandgap laser irradiation leads to significant redistributions of concentrations of As- and Se-centered structural units on the sample surface: the concentration of As – **Se** – Se and **As** – 3Se components increases while the **As**-rich Se – **As** – 2As and 2Se – **As** – As s.u. in the irradiated sample disappears. Such transformation implies an increase of the number of As – Se and Se – Se bonds and simultaneous decrease of the number of As – As bonds in the structure of the irradiated films. Taking into account the structure of realgar and pararealgar As_4Se_4 molecules and their building blocks, there is no direct evidence of a realgar-to-pararealgar photostructural transformation after sample irradiation in air.

Acknowledgments

The authors wish to thank Dr. M. Veres (Research Institute for Physics and Optics of the Hungarian Academy of Science) for his assistance with Raman monitoring of laser irradiation of the sample. R.H., N.P. and O.K. gratefully acknowledge the support of project 20100175 from the International Center of Theoretical Physics. The Materials Science Beamline is supported by the Ministry of Education of the Czech Republic under grant no. LC 06058 and by the Czech Grant Agency under contract number AS CR IAA1010143.

References

[1] A.V. Kolobov, J. Tominaga, J. Mater. Sci. Mater. Electron. 14 (2003) 677.
[2] K. Shimakawa, A. Kolobov, S.R. Elliott, Adv. Phys. 44 (1995) 475.
[3] K. Tanaka, Rev. Solid. State Sci. 4 (1990) 641.
[4] N.P. Eisenberg, M. Manevich, M. Klebanov, S. Shutina, V. Lyubin, Proc. SPIE Int. Soc. Opt. Eng. 2426 (1995) 235.
[5] M. Klebanov, S. Shutina, I. Bar, V. Lyubin, S. Rosenwaks, V. Volterra, Proc. SPIE Int. Soc. Opt. Eng. 2426 (1995) 198.
[6] H.M. Kim, J.W. Jeong, C.H. Kwak, S.S. Lee, Appl. Opt. 34 (26) (1995) 6008.
[7] R. Holomb, V. Mitsa, Solid State Commun. 129 (2004) 655.
[8] K.V. Adarsh, Ramakanta Naik, K.S. Sangunni, S. Kokenyesi, H. Jain, Alfred C. Miller, J. Appl. Phys. 104 (2008) 053501.
[9] R. Holomb, N. Mateleshko, V. Mitsa, P. Johansson, A. Matic, M. Veres, J. Non-Cryst. Solids 352 (2006) 1607.
[10] P. Krecmer, A.M. Moulin, R.J. Stephenson, T. Rayment, M.E. Welland, S.R. Elliott, Science 277 (1997) 1799.
[11] R. Holomb, V. Mitsa, P. Johansson, M. Veres, Phys. Status Solidi C 7 (3–4) (2010) 885.
[12] O. Kondrat, N. Popovich, R. Holomb, V. Mitsa, O. Petrachenkov, M. Koós, M. Veres, Phys. Status Solidi C 7 (3–4) (2010) 893.
[13] R. Holomb, M. Veres, V. Mitsa, J. Optoelectron. Adv. Mater. 11 (7) (2009) 917.
[14] R.A. Street, N.F. Mott, Phys. Rev. Lett. 35 (1975) 1293.
[15] R. Holomb, P. Johansson, V. Mitsa, I. Rosola, Philos. Mag. 85 (2005) 2947.
[16] D. Briggs, M.P. Seah, 2nd ed., Practical Surface Analysis, vol. 1, John Willey & Sons, 1993.
[17] J.J. Yeh, Atomic Calculation of Photoionization Cross-sections and Asymmetry Parameters, Gordon and Breach Science Publishers, Langhorne, PE, USA, 1993.
[18] J.J. Yeh, I. Lindau, At. Data Nucl. Data Tables 32 (1985) 1.
[19] C.D. Wagner, W.M. Riggs, L.E. Davis, J.F. Moulder, G.E. Muilenberg, Handbook of X-ray Photoelectron Spectroscopy, Perkin-Elmer Corp., Physical Electronics Division, Eden Prairie, Minnesota, USA, 1979.
[20] P.R. Sarode, K.J. Rao, M.S. Hegd, C.N.R. Rao, J. Phys. C. 12 (1979) 4119.
[21] T. Ueno, A. Odajima, Jpn. J. Appl. Phys. 20 (1981) L501.
[22] T. Ueno, Jpn. J. Appl. Phys. 22 (1983) 1469.
[23] M.K. Bahl, R.O. Woodall, R.L. Watson, K.J. Irgolic, J. Chem. Phys. 64 (1976) 1210.
[24] S. Krishnaswami, H. Jain, A.C. Miller, J. Optoelectron. Adv. Mater. 3 (3) (2001) 695.
[25] A.V. Kolobov, Y.P. Kostikov, S.S. Lantratova, V.M. Lyubin, Sov. Phys. Solid State 33 (1991) 444.
[26] T. Kitahara, T. Arai, Jpn. J. Appl. Phys. 18 (1979) 1635.
[27] H. Jain, S. Krishnaswami, A.C. Miller, P. Krecmer, S.R. Elliott, M. Vlcek, J. Non-Cryst. Solids 274 (2000) 115.
[28] K. Antoine, J. Li, D.A. Drabold, H. Jain, Mir. Vlchek, A.C. Miller, J. Non-Cryst. Solids 326&327 (2003) 248.

[29] K. Antoine, H. Jain, M. Vlchek, S.D. Senanayake, D.A. Drabold, Phys. Rev. B 79 (2009) 054204.
[30] M. Kalyva, A. Siokou, S.N. Yannopoulos, T. Wagner, J. Orava, M. Frumar, J. Non-Cryst. Solids 355 (2009) 1844.
[31] A. Kyono, Am. Mineral. 94 (2009) 451.
[32] H.A. Bullen, M.J. Dorko, J.K. Oman, S.J. Garrett, Surf. Sci. 531 (2003) 319.
[33] A. Kyono, M. Kimata, T. Hatta, Am. Mineral. 90 (2005) 1563.
[34] R. Holomb, V. Mitsa, P. Johansson, N. Mateleshko, A. Matic, M. Veresh, Chalc. Lett. 2 (2005) 63.
[35] R. Holomb, V. Mitsa, O. Petrachenkov, M. Veres, A. Stronski, M. Vlček, Phys. Status Solidi C 8 (9) (2011) 2705.